Available online at www.sciencedirect.com
ScienceDirect
Journal of Power Sources 175 (2008) 303–316
JOURNAL OF POWER SOURCES
www.elsevier.com/locate/jpowsour

Identification of the Hammerstein model of a PEMFC stack based on least squares support vector machines

Chun-Hua Li *, Xin-Jian Zhu, Guang-Yi Cao, Sheng Sui, Ming-Ruo Hu

Fuel Cell Research Institute, Shanghai Jiao Tong University, 800 Dongchuan Road, Shanghai 200240, PR China

Received 24 July 2007; received in revised form 15 September 2007; accepted 17 September 2007
Available online 21 September 2007

Abstract

This paper reports a Hammerstein modeling study of a proton exchange membrane fuel cell (PEMFC) stack using least squares support vector machines (LS-SVM). PEMFC is a complex nonlinear, multi-input and multi-output (MIMO) system that is hard to model by traditional methodologies. Due to the generalization performance of LS-SVM being independent of the dimensionality of the input data and the particularly simple structure of the Hammerstein model, a MIMO SVM-ARX (linear autoregression model with exogenous input) Hammerstein model is used to represent the PEMFC stack in this paper. The linear model parameters and the static nonlinearity can be obtained simultaneously by solving a set of linear equations followed by the singular value decomposition (SVD). The simulation tests demonstrate the obtained SVM-ARX Hammerstein model can efficiently approximate the dynamic behavior of a PEMFC stack. Furthermore, based on the proposed SVM-ARX Hammerstein model, valid control strategy studies such as predictive control, robust control can be developed.

Keywords: Hammerstein model; Proton exchange membrane fuel cell (PEMFC); Least squares support vector machines (LS-SVM); Model identification

1. Introduction

A fuel cell is an electrochemical device that converts the chemical energy of reactants (fuel and oxidant) directly into electricity energy. Water and heat are the only byproducts if hydrogen is used as the fuel source. The challenges of limited storage and adverse environmental impacts of conventional fossil fuels have raised interest and investigation in the fuel cell research. The proton exchange membrane fuel cell (PEMFC) is the focus of current efforts for its higher power density and faster start-up than other fuel cells [1]. An important tool in the fuel cell development is mathematical modeling. The results obtained from a reliable and effective model can be very useful to guide future research for fuel cell improvements and optimization. At the same time, the effective control of the PEMFC system also depends on the accurate mathematical model to simulate and predict its behavior under various operating conditions.

It is difficult to model the PEMFC system using traditional methods because of its nonlinear multi-input and multi-output (MIMO) dynamics. Over the last several decades, many researchers all over the world have made great progress on the PEMFC modeling. Most of the developed models distinctly describe internal microscopic characteristics, such as gaseous diffusion, thermal conduction, and liquid water transportation [2–4]. These models are very useful for cell design, but they are too complicated to be used in the design and analysis of a control system.

To meet the demands of developing valid control strategies, some researchers have attempted to establish novel fuel cell models by the statistical data-driven approach. The artificial neural network (ANN) was used to derive a solid oxide fuel cell (SOFC) model from the experimental data [5]. The direct methanol fuel cell (DMFC) voltage responses to cell current step changes are investigated with transfer function analysis in Ref. [6]. Jurado [7] identified a SISO model of SOFC using the nonlinear autoregressive exogenous

* Corresponding author. Tel.: +86 21 6293 3786 803; fax: +86 21 6293 2154.
E-mail address: viven_lch@sjtu.edu.cn (C.-H. Li).

0378-7753/$ – see front matter © 2007 Elsevier B.V. All rights reserved.
doi:10.1016/j.jpowsour.2007.09.049

Nomenclature

A	denominator of the ARX
A_{cell}	active area of single cell (cm^2)
A_s	cooling channel surface (m^2)
b	parametric coefficient (V)
B	numerator of the ARX
c_{O_2}	concentration of oxygen at the catalyst interface ($mol\,cm^{-3}$)
$c_{P,CL}$	Equivalent specific heat of cooling water ($J(kg\,K)^{-1}$)
$c_{P,FC}$	equivalent specific heat of overall fuel cell ($J(kg\,K)^{-1}$)
e	uncorrelated random error
E_{Nernst}	Nernst potential (V)
F	Faraday's constant ($96{,}485\,C\,mol^{-1}$)
$F_{in,a}$	inlet molar flow rate of anode ($kmol\,s^{-1}$)
$F_{in,c}$	inlet molar flow rate of compressor ($kmol\,s^{-1}$)
F_{O_2}	oxygen molar flow rate consumed by fuel cell ($kmol\,s^{-1}$)
$F_{valve,c}$	outlet molar flow rate of cathode exit valve ($kmol\,s^{-1}$)
ΔG	change in the free Gibbs energy ($J\,mol^{-1}$)
h_{FC}	internal convection coefficient ($W(m^2\,K)^{-1}$)
ΔH	change of the enthalpy ($J\,mol^{-1}$)
i	[O_2, N_2, vapor]
I	fuel cell current (A)
j	[H_2, vapor]
J	current density ($mA\,cm^{-2}$)
J_{max}	maximum current density ($mA\,cm^{-2}$)
k_{cath}	cathode valve constant ($(kmol\,kg)^{1/2}(atm\,s)^{-1}$)
k_{FC}	natural convection coefficient ($W\,K^{-1}$)
K_i	valve molar constant of i species ($kmol(s\,atm)^{-1}$)
m, n	order of the numerator and denominator in the transfer function of the ARX
m_{CL}	cooling water flow rate ($kg\,s^{-1}$)
M_{FC}	overall fuel cell mass (kg)
M_i	molar mass of i species ($kg\,kmol^{-1}$)
n_i	molar number of i species (kmol)
n_u, n_y	number of the input/output variables of model
N	number of sample data
N_{cell}	number of cells in a stack
P_{cath}, P_{an}	pressure in the cathode or anode (atm)
$P_{i,c}$, $P_{j,a}$	partial pressure of i or j species in the cathode or anode (atm)
$P_{sat,c}$	partial pressure of vapor with 100% relative humidity in the cathode (atm)
Q_{loss}	dissipated heat per cell
R	gas constant ($8.314\,J\,mol^{-1}\,K^{-1}$)
R_c	resistance to election flow (Ω)
R_M	resistance to proton flow (Ω)
ΔS	change of the entropy ($J\,mol^{-1}$)
$Stoi_{O_2}$	oxygen gas stoichiometry
T_1, T_2	inlet/exit temperature of cooling water (K)
T_{amb}	environmental temperature (K)
T_{ref}	reference temperature (K)
T_{stack}	fuel cell stack temperature (K)
u	input vector of the PEMFC stack
V_{cath}	volume of the cathode (m^3)
V_{cell}	average voltage of cells in a stack (V)
$X_{i,c}$	molar fraction of i species in the cathode
y	output vector of the PEMFC stack

Greek letters

α, β	Lagrange multipliers
δ	kernel width
γ	regularization parameter
η_{act}	activation overvoltage (V)
η_{con}	concentration overpotential (V)
η_{ohmic}	ohmic overvoltage (V)
τ_i	time constant of i species (s)
ξ_s	parametric coefficients based on experimental data ($s = 1, \ldots, 4$)

(NARX) approach. A nonlinear fuzzy model of a molten carbonate fuel cell (MCFC) stack was built with an identification method [8]. Most of them require the use of linearization techniques before executing the control strategies. As the complexity of the identified models increases, the variance on the obtained model parameters will increase as well.

The Hammerstein model [9,10] is a special kind of nonlinear systems where the nonlinear block is static and is followed by a dynamic linear system. Due to its particularly simple structure, Hammerstein system has been extensively studied in the context of system identification. Fuzzy Hammerstein models of a SOFC have been introduced in Refs. [11,12], and the parameters in the linear system and fuzzy system were ascertained separately. The least squares support vector machines (LS-SVM) [13,14] used for classification in various domains of pattern recognition, lately has handled regression problems successfully. Compared to the other modeling method, LS-SVM possesses prominent advantages: its generalization performance (i.e. error rates on test sets) either matches or is significantly better than that of competing methods, and more importantly, the performance does not depend on the dimensionality of the input data. The SVM has been used to develop the steady-state models (I–V characteristics) of the PEMFC and SOFC system [15,16].

In this paper, a SVM-ARX Hammerstein model is built to describe the dynamic characteristics of a PEMFC stack. The LS-SVM with a radial basis function (RBF) kernel is used for the representation of the static nonlinear block in the Hammerstein model. The dynamic linear part is realized by the linear autoregression model with exogenous input (ARX). The dynamic physical model of a 3 kW PEMFC stack provides the data used to identify the MIMO Hammerstein model. The linear model parameters and the static nonlinearity can be acquired simultaneously by solving a set of linear equations followed by the singular value decomposition (SVD).

The paper is organized as follows. In Section 2, the dynamic physical model of the PEMFC stack is presented. Section 3 develops the MIMO Hammerstein model using the LS-SVM approach. The modeling of the PEMFC stack based on the MIMO Hammerstein model is discussed in Section 4. Finally, conclusions are stated in Section 5.

2. PEMFC stack dynamic physical model

The basic fuel cell system structure with three main loops (the oxygen loop, the hydrogen loop, and the thermal loop) is shown in Fig. 1.

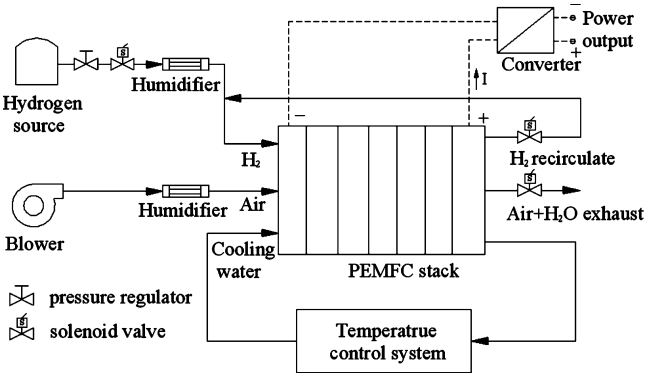

Fig. 1. Basic PEMFC system structure.

2.1. Steady-state electrochemical model

The steady-state electrochemical model can be used to predict fuel cell voltage output. The basic expression for the cell voltage can be defined by [17–19]:

$$V_{\text{cell}} = E_{\text{Nernst}} - \eta_{\text{act}} - \eta_{\text{ohmic}} - \eta_{\text{con}} \tag{1}$$

The Nernst potential V_{Nernst} represents the fuel cell open circuit voltage. This is given by:

$$E_{\text{Nernst}} = \frac{\Delta G}{2F} + \frac{\Delta S}{2F}(T_{\text{stack}} - T_{\text{ref}}) + \frac{RT_{\text{stack}}}{2F}(\ln(P_{\text{H}_2,\text{a}}) + 0.5\ln(P_{\text{O}_2,\text{c}})) \tag{2}$$

Using the standard pressure and temperature (SPT) value for ΔG, ΔS and T_{ref}, Eq. (2) can be simplified to [18,19]:

$$E_{\text{Nernst}} = 1.229 - 0.85 \times 10^{-3}(T_{\text{stack}} - 298.15) + 4.3085 \times 10^{-5} T_{\text{stack}} \times (\ln(P_{\text{H}_2,\text{a}}) + 0.5\ln(P_{\text{O}_2,\text{c}})) \tag{3}$$

The activation overpotential η_{act}, which takes into account both the anode and the cathode overpotential [18] can be calculated by:

$$\eta_{\text{act}} = -[\xi_1 + \xi_2 T_{\text{stack}} + \xi_3 T_{\text{stack}} \ln(c_{\text{O}_2}) + \xi_4 T_{\text{stack}} \ln(I)] \tag{4}$$

$$c_{\text{O}_2} = \frac{P_{\text{O}_2,\text{c}}}{5.08 \times 10^6 \exp(498/T_{\text{stack}})} \tag{5}$$

The ohmic overpotential results from the resistance to the electron transfer in the collecting plates and carbon electrodes, and the resistance to the proton transfer in the solid membrane. This can be represented using Ohm's law as [18]:

$$\eta_{\text{ohmic}} = I(R_{\text{c}} + R_{\text{M}}) \tag{6}$$

The concentration overpotential η_{con} due to the mass transport can be determined by [17,18]:

$$\eta_{\text{con}} = -b\ \ln\left(1 - \frac{J}{J_{\max}}\right) \tag{7}$$

As the cells are serially connected, the stack output voltage will be the summation of all the single cell output voltages. The cell voltage V_{cell} can be assumed to be the arithmetic average of cell voltages for a healthy stack.

2.2. Cathode and anode dynamic models

The following equations describe the variations of the gaseous species concentrations in the cathode compartment considering 100% humid gases [20–22]. The balance of oxygen and nitrogen allows us to write the following set of equations [20]:

$$\frac{\mathrm{d}n_{\text{O}_2}}{\mathrm{d}t} = 0.21F_{\text{in,c}} - F_{\text{O}_2} - X_{\text{O}_2,\text{c}}F_{\text{valve,c}} \tag{8}$$

$$\frac{\mathrm{d}n_{\text{N}_2}}{\mathrm{d}t} = 0.79F_{\text{in,c}} - X_{\text{N}_2,\text{c}}F_{\text{valve,c}} \tag{9}$$

$$\frac{\mathrm{d}n_{\text{vap}}}{\mathrm{d}t} = \frac{P_{\text{sat,c}}}{P_{\text{cath}} - P_{\text{sat,c}}}F_{\text{in,c}} - X_{\text{vap,c}}F_{\text{valve,c}} = \frac{X_{\text{vap,c}}}{1 - X_{\text{vap,c}}}F_{\text{in,c}} - X_{\text{vap,c}}F_{\text{valve,c}} \tag{10}$$

where:

$$F_{\text{O}_2} = \frac{N_{\text{cell}} \times I}{4/F}$$

$$X_{\text{O}_2,\text{c}} = \frac{P_{\text{O}_2,\text{c}}}{P_{\text{cath}}}$$

$$X_{\text{N}_2,\text{c}} = \frac{P_{\text{N}_2,\text{c}}}{P_{\text{cath}}}$$

$$X_{\text{vap,c}} = \frac{P_{\text{sat,c}}(T_{\text{stack}})}{P_{\text{cath}}}$$

The ideal gas law is used to calculate the pressure in the cathode:

$$P_{\text{cath}} = \frac{RT_{\text{stack}}}{V_{\text{cath}}}(n_{\text{O}_2} + n_{\text{N}_2} + n_{\text{vap}}) \tag{11}$$

The partial pressure of oxygen gas is:

$$P_{\text{O}_2,\text{c}} = \frac{RT_{\text{stack}}}{V_{\text{cath}}} n_{\text{O}_2} \tag{12}$$

Considering that the molar flow of any gas through the valve is proportional to its partial pressure, the following equation is derived:

$$\frac{X_{i,\text{c}} F_{\text{valve,c}}}{P_{i,\text{c}}} = \frac{k_{\text{cath}}}{\sqrt{M_i}} = K_i \tag{13}$$

Replacing n_{O_2} and $X_{\text{O}_2,\text{c}} F_{\text{valve,c}}$ in (8) by (12) and (13) respectively, taking the Laplace transform of both sides of (8) and isolating the oxygen partial pressure, yields the following expression:

$$P_{\text{O}_2,\text{c}} = \frac{1/K_{\text{O}_2}}{1 + \tau_{\text{O}_2} s}(0.21 F_{\text{in,c}} - k_r I) \tag{14}$$

where:

$$\tau_{\text{O}_2} = \frac{V_{\text{cath}}}{K_{\text{O}_2} RT_{\text{stack}}}$$

$$k_r == \frac{N_{\text{cell}} \times I}{4/F}.$$

The partial pressure of pure hydrogen gas with 100% relative humidity in the anode has the same derivation process as the oxygen partial pressure in the cathode. This is defined by:

$$P_{\text{H}_2,\text{a}} = \frac{1/K_{\text{H}_2}}{1 + \tau_{\text{H}_2} s}(F_{\text{in,a}} - 2k_r I) \tag{15}$$

2.3. Thermal model

The energy losses lead to a heat production. The heat is dissipated in the regions where the respective losses occur and is then evacuated from the cell through conduction to the bipolar plates and from there through convection to the ambient air and cooling liquid. The conduction phenomena within the plate are ignored when the stack can be treated as a lumped capacitance model and a constant bipolar plate temperature can be assumed [23].

Applying a basic energy balance for the bipolar plate allows us to express the evolution of the fuel cell temperature as [24]:

$$\frac{\text{d}T_{\text{stack}}}{\text{d}t} = \frac{1}{M_{\text{FC}} \times c_{\text{P,FC}}} \left[\underbrace{Q_{\text{loss}}}_{\text{Energy loss}} + \underbrace{m_{\text{CL}} \times c_{\text{P,CL}}(T_1 - T_2)}_{\text{Forced internal convection}} - \underbrace{k_{\text{FC}} \times (T_{\text{stack}} - T_{\text{amb}})}_{\text{Natural convection}} \right] \tag{16}$$

The internal heat source is generally composed of the entropy loss due to the electrical chemical reaction in both of the catalyst layers, the chemical energy required for oxygen and protons to overcome the barrier of the overpotentials and the latent heat of water condensation or evaporation [25,26]. The water phase-change heat transfer can be represented by the product of the latent heat of evaporation/condensation and the mass transfer rate [26]. The volume of the condensed/vaporized water is very small and the water phase-change enthalpy is negligible if compared with others [24,27,28]. The dissipated heat per cell can be written as:

$$Q_{\text{loss}} = \left(-\frac{\Delta H}{2F} - V_{\text{cell}} \right) \times I = \underbrace{\left(-\frac{\Delta H}{2F} - E_{\text{Nernst}} \right) \times I}_{\text{Entropy loss}} + \underbrace{(\eta_{\text{act}} + \eta_{\text{ohmic}} + \eta_{\text{con}}) \times I}_{\text{Overpotential loss}} \tag{17}$$

The exit temperature T_2 of cooling water is determined by the heat transferred to the cooling liquid along the cooling channels. Describing the heat transfer through forced internal convection, this can be expressed as [24]:

$$T_2 = T_{\text{stack}} - (T_{\text{stack}} - T_1) \exp\left(-\frac{A_{\text{s}} \times h_{\text{FC}}}{m_{\text{CL}} \times c_{\text{P,CL}}} \right) \tag{18}$$

The equivalent average convection coefficient h_{FC} can be determined through experimental Nusselt number correlations [29].

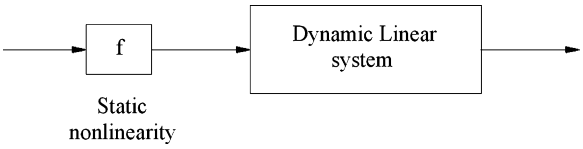

Fig. 2. Hammerstein system structure.

3. Nonlinear MIMO Hammerstein model

Hammerstein systems, in their most basic form, consist of a static memoryless nonlinearity, followed by a linear dynamical system as shown in Fig. 2. We will present some basic aspects of LS-SVM applied to static function estimation, the basic form of the MIMO SVM-ARX Hammerstein model and a method for the identification of the model in this section [30].

3.1. LS-SVM for function approximation

Assume a set of given input/output training data is given:

$$\{(u_t, y_t)\}_{t=1}^{N} \subset R^d \times R,$$

The regression model is defined as:

$$y_t = f(u_t) + e_t, \quad f : R^d \to R, \quad E[e_t] = 0, \quad E[e_t^2] = \sigma_e^2 < \infty,$$

where $u_1, \ldots, u_N$ are deterministic points, f is an unknown real-valued smooth function and $e_1, \ldots, e_N$ are uncorrelated random errors.

In order to estimate the nonlinear f using the LS-SVM [13], the following model is constructed:

$$f(u) = \omega^{\mathrm{T}}\varphi(u) + d, \quad \varphi : R^d \to R^{nH}, nH \to \infty, \tag{19}$$

where φ denotes a potentially infinite dimensional feature map. The quadratic loss function is selected in LS-SVM. The optimization problem of LS-SVM is formulated as:

$$\begin{aligned} &\min_{w,d,e} \zeta(w, e) = \frac{1}{2} w^{\mathrm{T}} w + \frac{\gamma}{2} \sum_{t=1}^{N} e_t^2 \\ &\text{s.t. } y_t = \omega^{\mathrm{T}}\varphi(u_t) + d + e_t, \quad t = 1, \ldots, N. \end{aligned} \tag{20}$$

In order to solve the constrained optimization problem, a Lagrangian is constructed as:

$$L(w, d, e; \alpha) = \zeta(w, e) - \sum_{t=1}^{N} \alpha_t (\omega^{\mathrm{T}}\varphi(u_t) + d + e_t - y_t), \quad \alpha_t \in R \tag{21}$$

where α_t ($t = 1, \ldots, N$) are the Lagrange multipliers. The conditions for optimality are given as:

$$\frac{\partial L}{\partial w} = 0 \to w = \sum_{t=1}^{N} \alpha_t \varphi(u_t), \tag{22}$$

$$\frac{\partial L}{\partial d} = 0 \to \sum_{t=1}^{N} \alpha_t = 0, \quad t = 1, \ldots, N, \tag{23}$$

$$\frac{\partial L}{\partial e_t} = 0 \to \alpha_t = \gamma e_t, \tag{24}$$

$$\frac{\partial L}{\partial \alpha_t} = 0 \to y_t = \omega^{\mathrm{T}}\varphi(u_t) + d + e_t, \quad t = 1, \ldots, N, \tag{25}$$

Substituting (22)–(24) into (25) yields the following set of linear equations:

$$\begin{bmatrix} 0 & 1_N^{\mathrm{T}} \\ 1_N & \Omega + \gamma^{-1} 1_N \end{bmatrix} \begin{bmatrix} d \\ \alpha \end{bmatrix} = \begin{bmatrix} 0 \\ y \end{bmatrix} \tag{26}$$

where:

$$y = [y_1, \ldots, y_N]^{\mathrm{T}} \in R^N,$$

$$1_N = [1, \ldots, 1]^{\mathrm{T}} \in R^N,$$

$$\alpha = [\alpha_1, \ldots, \alpha_N]^{\mathrm{T}} \in R^N,$$

$$\Omega_{i,j} = K(u_i, u_j) = \varphi(u_i,)^{\mathrm{T}}\varphi(u_j), \quad \forall i, j = 1, \ldots, N$$

The resulting LS-SVM model for function estimation can be evaluated at a new point u_* as:

$$\hat{y} = \hat{f}(u_*) = \sum_{t=1}^{N} \alpha_t K(u_t, u_*) + d \tag{27}$$

where (d, α) is the solution to (26).

The positive definite kernel function K is any symmetric function that satisfies Mercer's condition. For the choice of the kernel K see Ref. [31]. The RBF kernel function is used in this study because it tends to give good performance under general smoothness assumptions. The RBF kernel function is defined as:

$$K(u_i, u_j) = \exp\left(\frac{-||u_i - u_j||_2^2}{\delta^2}\right) \tag{28}$$

3.2. Basic form of MIMO Hammerstein model

For the linear dynamical part, we will assume a model structure of the MIMO ARX form [30]:

$$y_t = \sum_{i=1}^{n} A_i y_{t-i} + \sum_{j=0}^{m} B_j f(u_{t-j}) + e_t \tag{29}$$

where,

$$y_t, e_t \in R^{n_y}, \quad u_t \in R^{n_u}, \quad A_i \in R^{n_y \times n_y}, \quad B_j \in R^{n_y \times n_u}$$
$$t = 1, \ldots, N, \quad i = 1, \ldots, n, \quad j = 0, \ldots, m$$
$$f : R^{n_u} \to R^{n_u} : u \to f(u) = [f_1(u) \ldots f_{n_u}(u)]^T.$$

The so-called equation error e_t is assumed to be white. We have for every row s in (29), that

$$y_t(s) = \sum_{i=1}^{n} A_i(s, :) y_{t-i} + \sum_{j=0}^{m} B_j(s, :) f(u_{t-j}) + e_t(s), \qquad s = 1, \ldots, n_y \tag{30}$$

Substituting $f(u) = [f_1(u) \ldots f_{n_u}(u)]^{\mathrm{T}}$ in (30) leads to:

$$y_t(s) = \sum_{i=1}^{n} A_i(s, :) y_{t-i} + \sum_{j=0}^{m} \sum_{k=1}^{n_u} B_j(s, k) f_k(u_{t-j}) + e_t(s) \tag{31}$$

In order to apply LS-SVM function estimation, we replace $\sum_{k=1}^{n_u} B_j(s, k) f_k(u_{t-j})$ in (31) by $w_{j,s}^T \varphi(u_{t-j}) + d_{s,j}$, this reduces to:

$$y_t(s) = \sum_{i=1}^{n} A_i(s, :) y_{t-i} + \sum_{j=0}^{m} w_{j,s}^{\mathrm{T}} \varphi(u_{t-j}) + d_s + e_t(s), \quad \forall t, s \tag{32}$$

$$d_s = \sum_{j=0}^{m} d_{s,j}$$

The parametric component A of the linear dynamical system is naturally included in the LS-SVM framework. The optimization problem of LS-SVM is formulated as [30]:

$$\min_{w,A,B,d,e} \zeta(w_{j,s}, e) = \sum_{j=0}^{m}\sum_{s=1}^{n_y}\frac{1}{2}w_{j,s}^{\mathrm{T}}w_{j,s} + \frac{\gamma_s}{2}\sum_{s=1}^{n_y}\sum_{t=r}^{N}e_s(s)^2, \tag{33}$$

$$r = \max(m, n) + 1,$$

subject to (32) and $\sum_{t=1}^{N} w_{j,s}^{\mathrm{T}}\varphi(u_t) = 0$.

In order to solve the constrained optimization problem, a Lagrangian is constructed as:

$$L(w_{j,s}, d_s, A, e; \alpha, \beta) = \zeta(w_{j,s}, e) - \sum_{t=r}^{N}\sum_{s=1}^{n_y}\alpha_{t,s}\left(\sum_{i}^{n}A_i(s,:)y_{t-i} + \sum_{j=0}^{m}w_{j,s}^{\mathrm{T}}\varphi(u_{t-j}) + d_s + e_t(s) - y_t(s)\right)$$
$$-\sum_{j=0}^{m}\sum_{s=1}^{n_y}\beta_{j,s}\left(\sum_{t=1}^{N}w_{j,s}^{\mathrm{T}}\varphi(u_t)\right) \tag{34}$$

The conditions for optimality are given by:

$$\frac{\partial L}{\partial w_{j,s}} = 0; \quad \frac{\partial L}{\partial A_i(s,:)} = 0; \quad \frac{\partial L}{\partial d_s} = 0; \quad \frac{\partial L}{\partial e_t(s)} = 0; \quad \frac{\partial L}{\partial \alpha_{t,s}} = 0; \quad \frac{\partial L}{\partial \beta_{j,s}} = 0. \tag{35}$$

3.3. Identification of MIMO Hammerstein model

The aim of Hammerstein identification is to model the nonlinearity and to estimate the model parameters of the linear system from input/output measurements.

Given system (32), the LS-SVM estimates for the outputs at a new input u_* are given as:

$$\hat{y}_t(s) = \sum_{i=1}^{n}A_i(s,:)\hat{y}_{t-i} + \sum_{j=0}^{m}w_{j,s}^{\mathrm{T}}\varphi(u_*) + d_s, \quad t \geq r, \quad s = 1, \ldots, n_y, \tag{36}$$

$$w_{j,s}^{\mathrm{T}}\varphi(u_*) = \sum_{t=r}^{N}\alpha_{t,s}K(u_{t-j}, u_*) + \beta_{j,s}\sum_{t=1}^{N}K(u_t, u_*) \tag{37}$$

where

$a_{t,s}, t = r, \ldots, N, \quad s = 1, \ldots, n_y,$
$\beta_{j,s}, j = 0, \ldots, m, \quad s = 1, \ldots, n_y,$
$A_i, i = 1, \ldots, n,$
$d_s, s = 1, \ldots, n_y.$

These four parameters are obtained from the following set of linear equations [30]:

$$\begin{bmatrix} L_1 & & \\ & \ddots & \\ & & L_{n_y} \end{bmatrix}\begin{bmatrix} X_1 \\ \vdots \\ X_{n_y} \end{bmatrix} = \begin{bmatrix} R_1 \\ \vdots \\ R_{n_y} \end{bmatrix} \tag{38}$$

where:

$$L_s = \begin{bmatrix} 0 & 0 & 1_{N-r+1}^{\mathrm{T}} & 0 \\ 0 & 0 & y_p & 0 \\ 1_{N-r+1} & y_p^{\mathrm{T}} & k + \gamma_s^{-1}I & S \\ 0 & 0 & S^{\mathrm{T}} & T \end{bmatrix}$$

$$X_s = \begin{bmatrix} d_s \\ A_s \\ \bar{\alpha}_s \\ \bar{\beta}_s \end{bmatrix}, \quad y_p = \begin{bmatrix} y_{r-1} & y_r & \cdots & y_{N-1} \\ y_{r-2} & y_{r-1} & \cdots & y_{N-2} \\ \vdots & \vdots & \vdots & \vdots \\ y_{r-n} & y_{r-n+1} & \cdots & y_{N-n} \end{bmatrix}$$

$$R_s = \begin{bmatrix} 0 & 0 & y_{f,s}^{\mathrm{T}} & 0 \end{bmatrix}^{\mathrm{T}}, \quad y_{f,s}^{\mathrm{T}} = \begin{bmatrix} y_r(s)^{\mathrm{T}} & \dots & y_N(s)^{\mathrm{T}} \end{bmatrix}^{\mathrm{T}}$$

$$A_s = \begin{bmatrix} A_1(s,:)^{\mathrm{T}} & \dots & A_n(s,:)^{\mathrm{T}} \end{bmatrix}^{\mathrm{T}}$$

$$\bar{\alpha}_s = \begin{bmatrix} \alpha_{r,s} & \cdots & \alpha_{N,s} \end{bmatrix}^{\mathrm{T}}, \quad \bar{\beta}_s = \begin{bmatrix} \beta_{0,s} & \dots & \alpha_{m,s} \end{bmatrix}^{\mathrm{T}}$$

$$\Omega_{p,q} = \varphi(u_p)^{\mathrm{T}}\varphi(u_q), \quad k(p,q) = \sum_{j=0}^{m} \Omega_{p+r-j-1,q+r-j-1}$$

$$T = 1_N^{\mathrm{T}} \Omega 1_N 1_{m+1}, \quad S(p,q) = \sum_{t=1}^{N} \Omega_{t,r+p-q}$$

It is recommended to set $\gamma_1 = \gamma_2 = \cdots = \gamma_{ny}$. This will reduce the number of parameters to be tuned and speed up the estimation algorithm since $L_1 = L_1 = \cdots = L_{ny}$ needs to be calculated only once.

Estimates for the autoregressive matrices A_i, $i = 1, \dots, n$ are directly obtained from (38). For the training input sequence $[u_1, \dots, u_N]$, we have

$$\begin{bmatrix} B_0(1,:) \\ \vdots \\ B_m(1,:) \\ \vdots \\ B_0(n_y,:) \\ \vdots \\ B_m(n_y,:) \end{bmatrix} \times \begin{bmatrix} \hat{\underline{f}}^{\mathrm{T}}(u_1) \\ \vdots \\ \hat{\underline{f}}^{\mathrm{T}}(u_N) \end{bmatrix}^{\mathrm{T}} = \begin{bmatrix} \beta_{0,1} \\ \vdots \\ \beta_{m,1} \\ \vdots \\ \beta_{0,n_y} \\ \vdots \\ \beta_{m,n_y} \end{bmatrix} \sum_{t=1}^{N} \begin{bmatrix} \Omega_{t,1} \\ \vdots \\ \Omega_{t,N} \end{bmatrix}^{\mathrm{T}} + \begin{bmatrix} A_1 \\ \vdots \\ A_{n_y} \end{bmatrix} \times \begin{bmatrix} \Omega_{N,1} & \Omega_{N,2} & \cdots & \Omega_{N,N} \\ \Omega_{N-1,1} & \Omega_{N-1,1} & \cdots & \Omega_{N-1,N} \\ \vdots & \vdots & & \vdots \\ \Omega_{r-m,1} & \Omega_{r-m,2} & \cdots & \Omega_{r-m,N} \end{bmatrix}, \tag{39}$$

where

$$A_m = \begin{bmatrix} \alpha_{N,m} & \cdots & \alpha_{r,m} & & \\ & \alpha_{N,m} & \cdots & \alpha_{r,m} & \\ & & \ddots & & \ddots \\ & & & \alpha_{N,m} & \cdots & \alpha_{r,m} \end{bmatrix}, \quad m = 1, \dots, n_y,$$

with $\hat{\underline{f}}(u)$ an estimate for

$$\underline{f}(u) = f(u) - g \tag{40}$$

and g a constant vector such that:

$$\sum_{j=0}^{m} B_j g = [d_1 \cdots d_{n_y}]^{\mathrm{T}} \tag{41}$$

Estimates for $\underline{f}$ and the B_j, $j = 0, \dots, m$, can be obtained through a rank-n_u approximation of the right-hand side of (39), for instance using a singular value decomposition [32]. From $\underline{f}$ in (40) and g in (41), finally, an estimate for the nonlinear function f can be obtained.

Table 1
Model parameters

Parameter	Value
N_{cell}	28
A_{cell} (cm^2)	400
K_{H_2} ($kmol(s\,atm)^{-1}$)	4.22×10^{-5}
τ_{H_2} (s)	3.37
K_{O_2} ($kmol(s\,atm)^{-1}$)	2.11×10^{-5}
τ_{O_2} (s)	6.74
k_{FC} ($W\,K^{-1}$)	0.7
J ($mA\,cm^{-2}$)	260–580
$Stoi_{O_2}$	1.2–2.5
M_{FC} (kg)	8.8
$c_{P,FC}$ ($J(kg\,K)^{-1}$)	920
$c_{P,CL}$ ($J(kg\,K)^{-1}$)	4180
h_{FC} ($W(m^2\,K)^{-1}$)	3990
A_s (cm^2)	820
m_{CL} ($kg\,s^{-1}$)	0.01–0.03
T_1 (K)	323.15

Mean squared error (MSE) is employed here to evaluate modeling results:

$$\mathrm{MSE} = \frac{1}{N}\sum_{t=1}^{N}(\hat{y}_t - y_t)^2 \tag{42}$$

where $\hat{y}_t$ is the predictive output of the Hammerstein model and y_t is the output of the real PEMFC stack.

Now the dynamic and static parts of MIMO Hammerstein model have been identified. The model will be adopted to represent the dynamic nonlinear characteristics of the PEMFC stack based on simulation data.

4. Results on the modeling of the PEMFC stack

The modeling of the PEMFC stack based on the Hammerstein model is developed in this section. In this modeling procedure, the relationship between inputs and outputs of the PEMFC stack can be emphasized while the sophisticated inner structure is ignored. The output voltage of the PEMFC stack depends on many operation parameters such as: current I, oxygen partial pressure $P_{O_2,c}$, hydrogen partial pressure $P_{H_2,a}$, and stack temperature T_{stack} with the assumption that channel gas is fully saturated and membrane is fully humidified. In engineering application, hydrogen flow rate $F_{in,a}$ must be tuned according to $|P_{cath} - P_{an}|$ in order to minimize the pressure difference between the cathode and the anode and protect the membrane against cracking. $P_{H_2,a}$ actually depends on $F_{in,c}$ by a simple feedforward control. Based on above description, the voltage of the PEMFC stack can be controlled by $P_{O_2,c}$ and T_{stack} through two manipulated variables: the oxygen gas stoichiometry $Stoi_{O_2} = (0.21F_{in,c})/F_{O_2}$, and the cooling liquid flow rate m_{CL}. The current I is considered as a system disturbance. Consequently, the PEMFC stack is modeled with three inputs $u = [I, Stoi_{O_2}, m_{CL}]^T$ and two outputs $y = [P_{O_2,c}, T_{stack}]^T$.

The duty of modeling the PEMFC stack is to set up the relations between input vector u and output vector y based on the Hammerstein model using a set of sample data $\{u_t, y_t\}$, $t = 1, \ldots, N$. In the following, the training process of the Hammerstein model is presented firstly, and then the model are utilized to predict outputs of the PEMFC stack.

4.1. Training the Hammerstein model

In general, steps used in training the Hammerstein model based on LS-SVM include: choosing and preprocessing experimental data, and selecting the optimal SVM-ARX Hammerstein model parameters.

4.1.1. Preparing the training data set

In our study, a 3 kW PEMFC stack is considered to the prototype of this modeling. The dynamic physical model of the PEMFC stack is built up according to Section 2 using MATLAB to generate the data set required for the identification of the Hammerstein model. Pure hydrogen and air are used as the fuels for the anode and the cathode respectively. The configuration and operating conditions of this stack are shown in Table 1. For the purpose of identification, the dynamic physical model was excited with uniformly random input signals including the current density (260–580 $mA\,cm^{-2}$), the oxygen gas stoichiometry (1.2–2.5) and the cooling liquid flow (0.01–0.03 $kg\,s^{-1}$). The fourth-order Runge-Kutta method was used to find the numerical solution to the dynamic physical model in the simulation.

The stack temperature usually needs more than 500 s to achieve steady state and oxygen partial pressure just needs less than 50 s according to the same inputs. In order to reduce the sample data and acquire an adequately short online predicting time, the oxygen partial pressure and the stack temperature are sampled using different time intervals under the conditions of keeping a certain prediction precision. A set of 1000 training data are collected for $P_{O_2,c}$ and T_{stack} respectively from the simulation excited with the same input series. The first 900 data are used to identify the static nonlinearity and the transfer function of the linear system, while the remaining 100 data are used for validation purposes.

All chosen training data are normalized to [0,1] by (43) which can accelerate the training speed.

$$u_t'(v) = \frac{u_t(v) - u_{\min}(v)}{u_{\max}(v) - u_{\min}(v)}, \quad \begin{matrix} t = 1, \ldots, N \\ v = I, \mathrm{Stoi}_{O_2}, m_{CL} \end{matrix} \tag{43}$$

4.1.2. Selection of the optimal model parameters

The key to obtaining a highly accurate MIMO Hammerstein model is to choose a proper parameter set. There are four parameters in this modeling process needing to be tuned: γ in Eq. (33), which determines the trade-off between minimizing training errors and minimizing model complexity; δ in Eqs. (28) and (37), which directly influences the number of initial eigenvalues/eigenvectors and the fitting level of the static model; m and n in Eq. (29), both of which decide the dynamic performance of the identified Hammerstein model. As a general rule, a slight overestimation of m and n is, as in the linear case, not a problem [30].

We firstly tune γ and δ with fixed m and n, and then adjust m and n with the fixed γ and δ found in the former step. We can rapidly tune the four parameters using the 10-fold cross-validation method [15,16], which is often used in practical applications. The final optimal parameters are: $\gamma = 50$, $\delta = 0.5$, $m = 4$ and $n = 8$.

4.2. Predicting with the Hammerstein models

The linear system (38) is solved for d, A, α, and β. An SVD of the right hand side of (39) is thereafter performed to obtain estimates for the linear system B and the static nonlinearity f as shown in Fig. 3. This identified model can be used to predict the dynamic characteristics of the PEMFC stack by Eq. (36). The MSE obtained in test process of P_{O_2} and T_{stack} with maximum values of 1 atm and 372 K is 0.0002035 and 0.1201 respectively. Off-line optimizing of the Hammerstein model took 23 min on a Pentium IV 3.0 GHz computer with 1 GB RAM, but the predicting time was no more than 0.2 s.

Nine hundred data of $\{f, u\}$ is used to develop the inverse of the static nonlinearity in the Hammerstein model [9,33] using LS-SVM with f as inputs, u as outputs, $m = 0$ and $n = 0$. The MSE of 100 test data of $\{I, \mathrm{Stoi}_{O_2}$, and $m_{CL}\}$ with maximum values of 232 A, 2.5 and 0.03 kg s^{-1} is 0.5032, 2.0493e−4, and 4.7205e−8 respectively.

Ten continuous random input signals are fed into the dynamically physical model and the identified Hammerstein model. The sample data of input signals and the data obtained by the inverse of the nonlinearity are displayed in Fig. 4. The comparison between predicted and experimental dynamic output curves of P_{O_2} is given in Figs. 5 and 6 presents the predicted and experimental dynamic outputs of T_{stack}. Figs. 5 and 6 show high fitting accuracy of the SVM-Hammerstin model for the dynamic behavior of the PEMFC stack.

In order to observe the predicting precision when using different sample intervals to these two output variables, the predicted voltage outputs and experimental voltage outputs are shown in Fig. 7. The stack temperature keeps invariable in its sample interval.

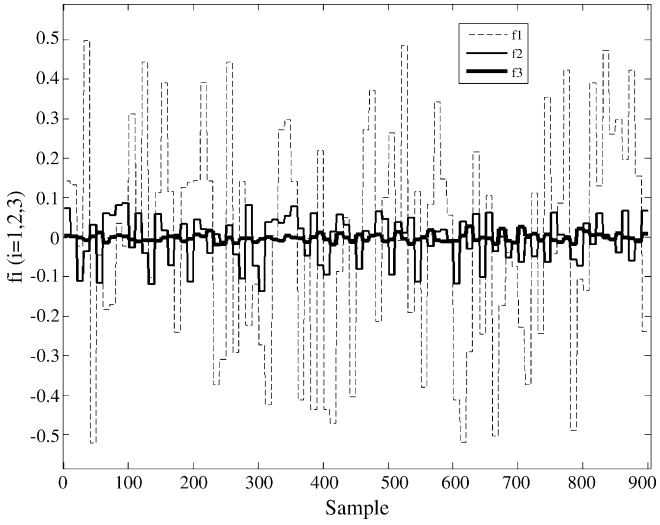

Fig. 3. Outputs of the nonlinearity for 900 training data.

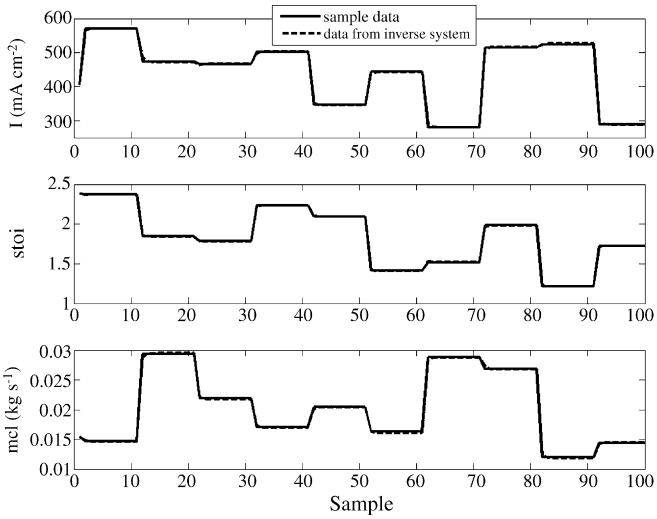

Fig. 4. Ten continuous random inputs and the data from inverse system.

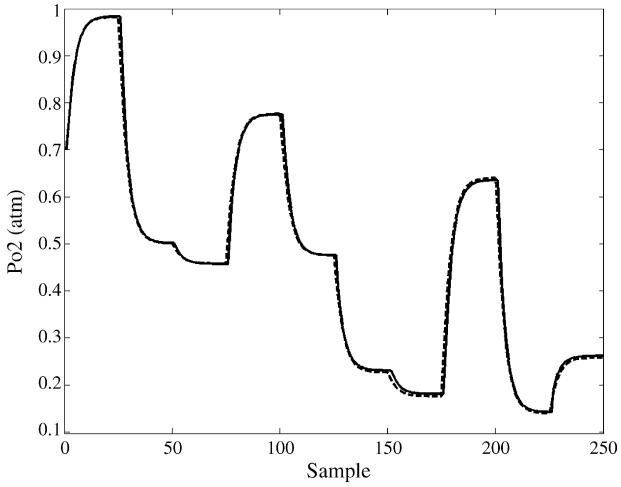

Fig. 5. Dynamic outputs of oxygen partial pressure.

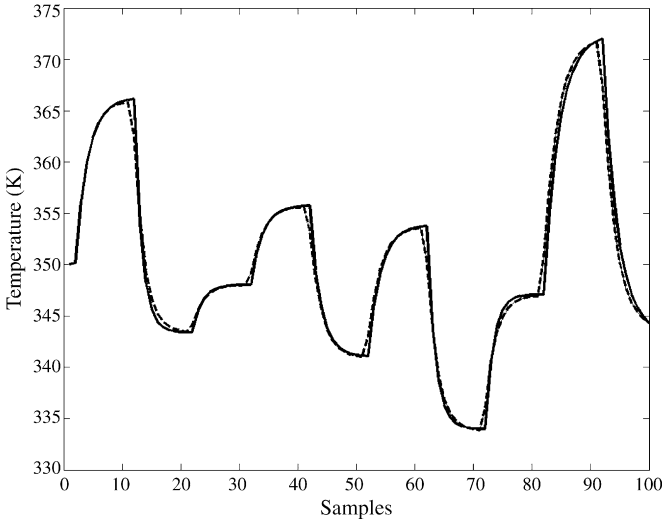

Fig. 6. Dynamic outputs of stack temperature.

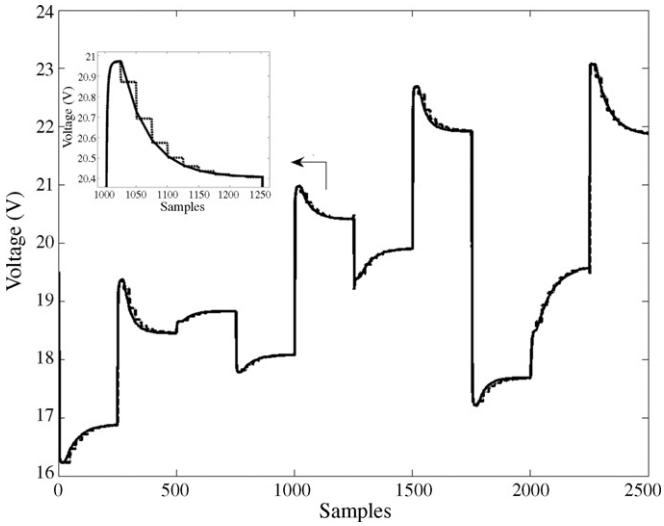

Fig. 7. Dynamic outputs of stack voltage.

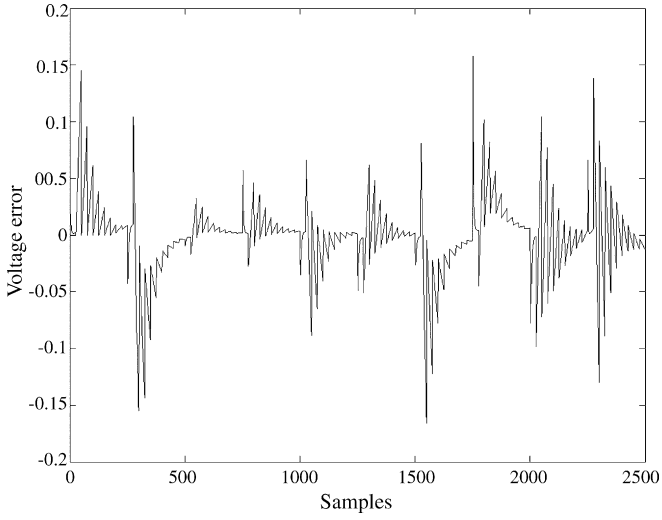

Fig. 8. Output errors of stack voltage.

The voltage error is shown in Fig. 8. The MSE of the PEMFC stack voltage with the maximum value of 23 V is 0.0012 which guarantees a good predicting performance of the Hammerstein model.

5. Conclusions

To facilitate valid control strategy design and analysis, a MIMO Hammerstein model of a PEMFC stack is built up using LS-SVM in this paper. The identification of the static nonlinearity and dynamic linear model parameters is achieved at the same time by solving a set of linear equations followed by the singular value decomposition, which ensures the parametric consistency and the accurate description of the model. The identified MIMO Hammerstein model of PEMFC is more attractive in that it avoids using complicated differential equations to describe the dynamic characteristics of a PEMFC stack. The linear part of the Hammerstein model can be utilized directly to search optimal operating variables by control strategies. In order to implement the control scheme, we have presented a good representation of the inverse of the nonlinearity part in the Hammerstein model. In the future, some control scheme studies such as predictive control and robust control can be developed based on the Hammerstein model.

Acknowledgement

This work is supported by the National Natural Science Foundation (NNSF) of China (Grant 20576071).

References

[1] A. Haddad, R. Bouyekhf, A.E. Moudni, M. Wack, J. Power Sources 163 (2006) 420–432.
[2] S.A. Baghdadi, A.R. Maher, S.A. Janabi, A.K. Haroun, J. Renew. Energy 32 (2007) 1077–1101.
[3] D.F. Cheddie, N.D.H. Munroe, J. Power Sources 160 (2006) 215–223.
[4] T. Murahashi, M. Naiki, E. Nishiyama, J. Power Sources 162 (2006) 1130–1136.
[5] J. Arriagada, P. Olausson, J. Power Sources 112 (2002) 54–60.
[6] U. Krewera, K. Sundmachera, J. Power Sources 154 (2005) 153–170.
[7] F. Jurado, Fuel cells 5 (2005) 105–114.
[8] F. Yang, X.-J. Zhu, G.-Y. Cao, J. Power Sources 166 (2007) 354–361.
[9] K.P. Fruzzetti, A. Palazoglu, K.A. Mcdonald, J. Process Control 7 (1996) 31–41.
[10] K.H. Chan, J. Bao, W.J. Whiten, J. Process Control 16 (2006) 659–670.
[11] F. Jurado, J. Power Sources 158 (2006) 245–253.
[12] F. Jurado, M. Ortega, Electr. Power Compon. Syst. 34 (2006) 587–602.
[13] J.A.K. Suykens, J. Vandewalle, Neural Process. Lett. 9 (3) (1999) 293–300.
[14] Y.B. Dibike, S. Velickov, D. Solomatine, M.B. Abbott, J. Comput. Civil Eng. 15 (3) (2001) 208–216.
[15] Z.-D. Zhong, X.-J. Zhu, G.-Y. Cao, J. Power Sources 160 (1) (2006) 293–298.
[16] H.-B. Huo, X.-J. Zhu, G.-Y. Cao, J. Power Sources 162 (2) (2006) 1220–1225.
[17] J.M. Correa, F.A. Farret, L.N. Canha, M.G. Simoes, IEEE Trans. Ind. Electron. 51 (2004) 1103–1112.
[18] R.F. Mann, J.C. Amphlett, M.A.I. Hooper, H.M. Jensen, B.A. Peppley, P.R. Roberge, J. Power Sources 86 (2000) 173–180.
[19] J.J. Baschuk, X. Li, J. Power Sources 86 (2000) 181–196.
[20] S. Caux, J. Lachaize, M. Fadel, P. Schott, L. Nicod, IEEE Vehicle Power and Propulsion Conference, 2005, pp. 597–602.
[21] J. Padulles, G.W. Ault, J.R. Mcdonald, J. Power Sources 86 (2000) 495–500.
[22] M.Y.E. Sharkh, A. Rahman, M.S. Alam, P.C. Byrne, A.A. Sakla, T. Thomas, J. Power Sources 138 (2004) 199–204.
[23] F. Incropera, D. DeWitt, Introduction to Heat Transfer, John Wiley and Sons, New York, 1996.
[24] F. Grasser, A. Rufer, Presented at: The Fourth Power Conversion Conference, 2007, pp. 77–91.
[25] Y. Shan, S.Y. Choe, J. Power Sources 158 (2006) 274–286.
[26] J.J. Hwang, J. Power Sources 164 (2007) 174–181.
[27] M. DeFrancesco, E. Arato, J. Power Sources 108 (2000) 41–52.
[28] T. Araki, H. Koori, T. Taniuchi, K. Onda, J. Power Sources 152 (2005) 60–66.
[29] W. Kays, M. Crawford, Convection Heat and Mass Transfer, McGraw-Hill, New York, 1980.
[30] I. Goethals, K. Pelckmans, J.A.K. Suykens, B.D. Moor, Automatica 41 (2005) 1263–1272.
[31] B. Scholkopf, A. Smola, Learning with Kernels, MIT Press, Cambridge, MA, 2002.
[32] J.C. Gomez, E. Baeyens, J. Process Control 14 (2004) 685–697.
[33] A.L. Cervantes, O.E. Agamennoni, J.L. Figueroa, J. Process Control 13 (2003) 655–666.